



Cite this: *CrystEngComm*, 2017, 19, 608

Received 23rd November 2016,
Accepted 22nd December 2016

DOI: 10.1039/c6ce02436j

www.rsc.org/crystengcomm

Single crystals of metal–organic framework-199 are successfully synthesized in a hydrogel medium using a reaction–diffusion framework. This method is rapid, efficient, scalable, and environmentally friendly. Control over the size, dispersity and the morphology of the crystals is achieved and several key parameters in the mechanism of crystal growth are elucidated.

Metal–organic frameworks (MOFs) are an established class of highly porous and crystalline materials composed of organic linkers and inorganic clusters connected *via* strong chemical bonds.^{1–5} As a result of their high surface area and compositional versatility, MOF structures have been used in many applications ranging from gas storage and separation, catalysis and sensing to adsorption-driven heat pumps.^{6–9} Traditionally, MOFs are prepared through solvothermal methods, but alternative synthetic strategies have been developed based on exploiting conventional electric or microwave heating, electrochemistry, mechanochemistry, and ultrasonication.^{10–12} On the other hand, room temperature synthesis through fast precipitation (nano-size crystals of MOFs) or slow diffusion (single crystals) are used to a much lesser extent.^{13,14} In most of these methods, an organic solvent is needed. In the few reports, in which aqueous or solvent-free media are employed, high temperatures and/or continuous energy input are necessary to realize the targeted material.^{15–18} However, among the tens of thousands of MOF structures reported to date, there are only a handful of examples of synthesis employing organic solvent-free techniques at room temperature.^{13,14,19} Therefore, as a matter of necessity, the development of novel synthetic routes to MOFs, which take into consideration environmental issues, safety hazards, and energy costs prior to implementing these materials in an industrial setting are highly sought after. While the synthesis,

Synthesis, size and structural evolution of metal–organic framework-199 *via* a reaction–diffusion process at room temperature†

Mazen Al-Ghoul,* Razan Issa and Mohamad Hmadeh*

characterization, and application of new MOF structures are profusely published, a fundamental understanding^{20–22} of MOF crystal formation mechanisms is still lagging and investigations concerning the different parameters governing the synthetic procedures (*i.e.* the concentrations of the starting materials, the type of metal sources or solvents, as well as the pH and temperature) are only intermittently reported.^{23–26}

MOF-199, $\text{Cu}_3(\text{BTC})_2$ (BTC = benzene-1,3,5-tricarboxylate), also known as HKUST-1,²⁷ is one of the most studied metal–organic framework materials due to its potential application in gas sorption, storage, and separation. Because control over the extent of size and shape of such a MOF is achievable through an interplay of the chemical reaction route with the kinetics of crystal nucleation and growth during synthesis,

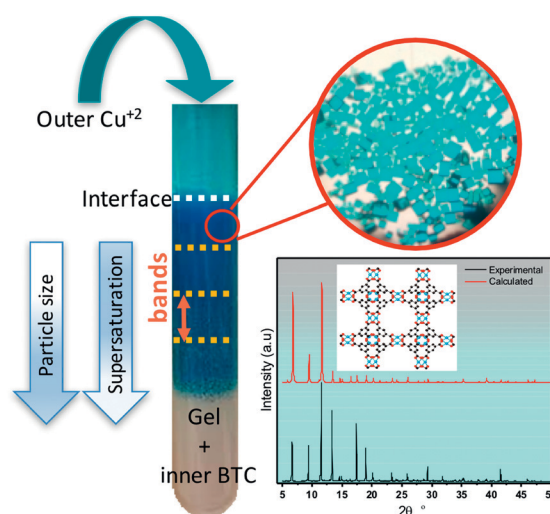


Fig. 1 Synthesis of MOF-199 crystals using a reaction–diffusion framework (RDF). Starting at the interface and down the tube, crystals with different sizes are extracted from equally sized (5 mm thickness) and consecutive region-bands. The zoom-in optical image reveals blue cubic crystals identified as MOF-199 by the comparison of the PXRD patterns of the as-synthesized crystals (black) with the calculated pattern of MOF-199 (red).

Department of Chemistry, Faculty of Arts and Sciences, American University of Beirut, P.O. Box 11-0236 Riad El Solh, Beirut 1107-2020, Lebanon.

E-mail: mazen.ghoul@aub.edu.lb, mohamad.hmadeh@aub.edu.lb

† Electronic supplementary information (ESI) available. See DOI: 10.1039/c6ce02436j

we employ a reaction–diffusion framework (RDF) that exploits such coupling and provides a remarkable grip on size control and monodispersity.²⁸ This coupling essentially relies on the strong dependence of nucleation, growth, and ripening of the crystalline solid on supersaturation. Moreover, the RDF constitutes a facile and rapid method of synthesizing MOF-199 at room temperature and consists of a precipitate system designed by diffusing Cu^{2+} cations (the outer electrolyte solution) into an agar gel matrix that is loaded with the BTC organic linker (the inner electrolyte solution). The gel network traps the crystal nuclei and prevents crystal sedimentation thereby fostering a three-dimensional crystal growth. Furthermore, although the agar eliminates convection and stabilizes the depletion zones around growing crystals, it does not restrict macromolecular diffusion; and by inhibiting the rate of nucleation and growth, it leads to better quality crystals with local uniform size distributions.^{29,30} Due to the reactants being initially separated and poured on top of each other, a concentration gradient is established, leading to a propagating and decreasing supersaturation wave starting at the gel–outer solution interface and extending down the reaction tube (Fig. 1). While nucleation dominates near the interface where supersaturation is at its highest, growth takes over further down the reaction tube where supersaturation is considerably lower. This consequently leads to a gradient in the crystal size at different heights along the reaction tube with the smallest crystals near the interface.³¹ The size distribution as a function of distance is generally nonlinear and depends on the specific experimental conditions and on the molecular, chemical and transport characteristics of the reactants and products. Therefore, by employing this reaction–diffusion method, we are able to study the control of both the morphology and size of the resulting MOF-199 particles through adjustment of the concentration of the reactants, the thickness of the gel, and the reaction temperature. Furthermore, this method enables the elucidation of the fundamental physico-chemical parameters that govern the crystallization process of MOF-199.

As schematically illustrated in Fig. 1, the synthesis medium consists of a gel matrix (1% agar) occupying about two-thirds of a Pyrex tube in which BTC is immobilized. On top of the gel, an aqueous solution of Cu^{2+} is poured (see the ESI† for more details). Under static conditions, diffusion of Cu^{2+} cations into the gel matrix results in the growth of blue cubic crystals in the gel. A small volume of ethanol (*ca.* 10%) is added to the outer and inner solutions. Without ethanol, the MOF-199 cubic crystals could not be obtained. It is reported that the interactions between the solvent molecules and BTC molecules are weakened with the increasing ethanol content; consequently, this reduction in the interaction favors the coordination of the organic ligand with metal ions, thus promoting MOF formation in a water/ethanol mixture as the ethanol content reaches a certain value.³² Interestingly, this synthesis process can be scaled up by simply using a larger container (*e.g.* 1 L) without affecting the quality of the crystals (Fig. S1†). The gel layer is then easily glided out of

the tube by a spatula and cut into consecutive and equally sized (5 mm thickness) bands. The blue crystals (yield of *ca.* 95%) are subsequently extracted from each band by dissolving the gel in hot water (60 °C) followed by centrifugation, washing with water and dimethylformamide several times, and freeze-drying for 12 hours. The obtained sample is then subjected to powder X-ray diffraction (PXRD), high-resolution scanning electron microscopy (HRSEM), thermogravimetric analysis (TGA) and N_2 sorption measurements. PXRD patterns are collected using a Bruker D8 Discover diffractometer with $\text{Cu-K}\alpha$ radiation and are shown in Fig. 1. All peaks perfectly match the cubic structure of MOF-199 with a lattice parameter of $a = 26.30 \text{ \AA}$ and no additional peaks are observed indicating the high purity of our sample. The N_2 isotherm of the activated crystals (Fig. S2†) is measured using a Micromeritics ASAP 2420 analyzer and the BET surface area is calculated to be $1250 \text{ m}^2 \text{ g}^{-1}$. This value is in good agreement with the reported values for MOF-199, which demonstrates that the growth of the crystal within the gel matrix did not affect the texture and structural properties of the framework. This was further confirmed by the thermogravimetric analysis (TGA) of the precipitates of the activated sample using a TG 209 F1 Iris (Netzsch, Germany), which shows the complete removal of the gel from the crystals (Fig. S3†). The morphology of the gold-coated samples was examined using a (Tescan Mira) scanning electron microscope. By changing the type of copper salts, two different morphologies are observed. While the cubic crystals of MOF-199 (Fig. 1) are obtained by using copper acetate as the outer electrolyte, copper nitrate leads to the formation of polyhedron-like crystals (Fig. S4 and S5†). Interestingly, no additives or modulators are needed in our synthesis route to produce these two crystal shapes at room temperature.

Different experimental parameters for the synthesis of the MOF-199 crystals are investigated. Starting from copper acetate as the outer electrolyte (resulting in cubic crystals), the effect of the BTC concentration, gel concentration and temperature on the size distribution within the gel matrix are studied. To this end, different experiments are carried out in which one of the parameters is varied while the other two are kept fixed. Tubes are divided into bands of 0.5 cm thickness each (as shown in Fig. 1), from which the crystals are extracted from the gel and then analyzed by PXRD and HRSEM. The average crystal size is computed as the mean of 50–100 crystals per band. Fig. 2A represents typical SEM images of 4 consecutive bands for a given inner and outer concentration of the reactants. When different concentrations of the inner electrolyte are used (5 mM, 10 mM, 20 mM and 50 mM), in 1% gel and 100 mM $\text{Cu}(\text{OAc})_2$ to ensure high initial supersaturation, the obtained distributions of crystal sizes are presented in Fig. 2B. It is clear that there is an almost-linear strong concentration dependence on the crystal size of MOF-199. The effect on the crystal size is represented as a bar graph of the resulting smallest and largest crystal sizes in Fig. 2D and S6†. At a low concentration of BTC (5 mM), we obtained the smallest size gradient (slope) of *ca.* $25 \mu\text{m cm}^{-1}$

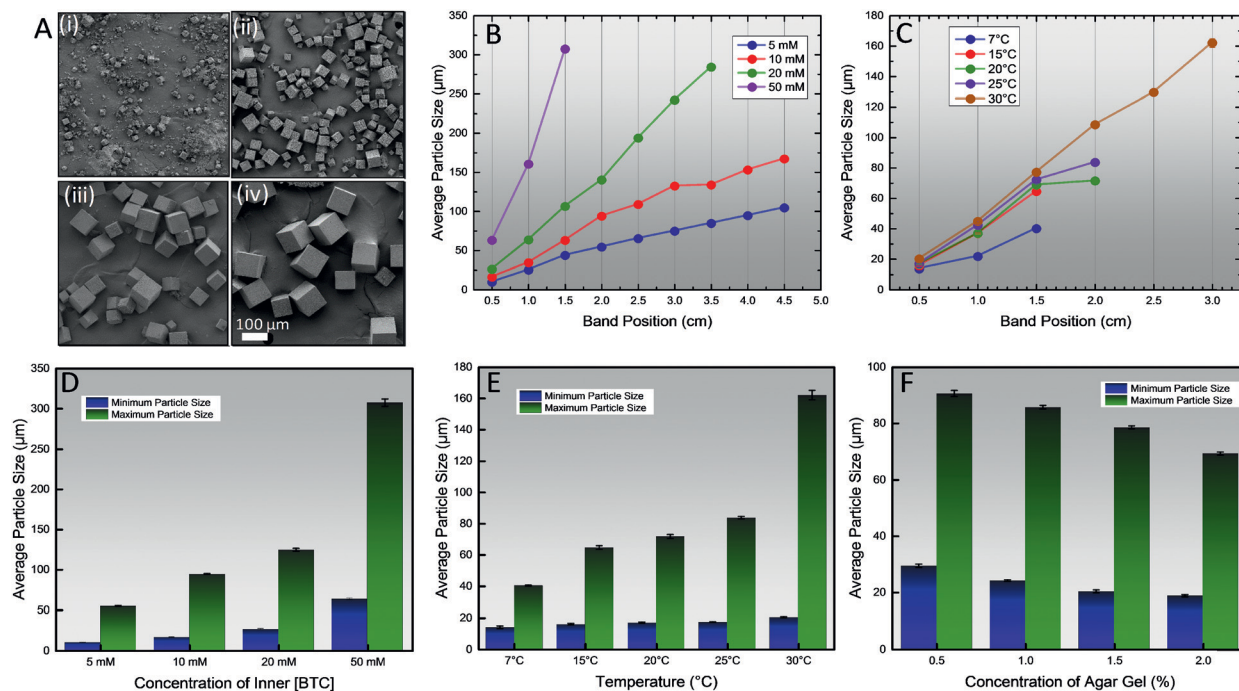


Fig. 2 Scanning electron microscopy images of MOF-199 crystals obtained from four consecutive different bands (0.5 cm thickness) with $[\text{Cu}^{2+}] = 100 \text{ mM}$ and $[\text{BTC}] = 20 \text{ mM}$ at 25°C . (A) Crystal size distributions at different concentrations of BTC at fixed outer $[\text{Cu}^{2+}] = 100 \text{ mM}$ and after 24 h (B) and at different temperatures for $[\text{BTC}] = 10 \text{ mM}$ and $[\text{Cu}^{2+}] = 100 \text{ mM}$ after 24 h. (C) Bar graph indicators for the smallest and largest crystal sizes achieved for the effect of different inner [BTC], (D) different temperatures (E) and different gel concentrations (F).

with cubic sizes in the range of 10–55 μm . However, for a concentration of $[\text{BTC}] = 50 \text{ mM}$, the crystal size reaches 310 μm with a steep size gradient of *ca.* 220 $\mu\text{m cm}^{-1}$. This concomitant increase of the minimum and maximum size of the MOF cubes with the increase of the inner [BTC] is a characteristic of the RDF, whereby the supersaturation gradient plays the major role in the spatial variation of the particle sizes. The temperature has also a noticeable effect on the particle size distribution as shown in Fig. 2C and E and S7.† For a $[\text{BTC}] = 10 \text{ mM}$ and $[\text{Cu}^{2+}] = 100 \text{ mM}$ the gradient of the cubic size changes from *ca.* 32 $\mu\text{m cm}^{-1}$ at a temperature of 7°C to a *ca.* 55 $\mu\text{m cm}^{-1}$ at 30°C . The effect of temperature on the extent of reaction–diffusion is also noticeable. For example, at 7°C the reaction front does not reach beyond the third band after 24 h whereas it reaches the sixth band at 30°C . This is due to the faster diffusion of the reaction front at higher temperatures (and at a higher difference between the inner and outer concentrations). The concentration of the agar gel is an important parameter in the RDF process. This effect is investigated at different concentrations of the gel (0.5%, 1%, 1.5% and 2%) while keeping the BTC and $\text{Cu}(\text{OAc})_2$ constant at 20 mM and 100 mM, respectively. The HRSEM images and the particles size distribution of the different samples are presented in Fig. S8† and the size indicators in Fig. 2F reveal a clear effect of the gel concentration on the size of the crystals whereby the largest size is achieved at the lowest gel concentration. This trend correlates with the fact that when the average pore size of the agar gel decreases as concentration increases, the rate of nucleation and growth

of crystals within these pores decreases.^{33,34} It is noteworthy that the crystals of different sizes that are extracted from different bands in a given tube exhibit almost identical physical properties as seen in the PXRD, TGA and BET measurements in Fig. S9.†

Reaction–diffusion in gel matrices also provides a convenient framework to study the crystal evolution of MOF-199 due to the considerable hindering of the rates of nucleation and growth when compared to those in various condensed media. For this study, MOF-199 is prepared in 5 different identical tubes with a given inner and outer concentration. The crystals are then respectively extracted from the gel–outer interface of each tube at different times (6 s, 10 s, 5 min, 30 min and 2 h) by discarding the outer electrolyte. The investigation of the interface region, where nucleation dominates, allows us to capture the transition to cubic MOF-199 crystals. In Fig. 3, the HRSEM reveals that the formation of the first perfect cubic crystals is fast (*ca.* 10 s) and preceded by the instantaneous homogeneous nucleation and growth of nanospheroids of a maximum size of *ca.* 150 nm. The PXRD patterns of the solids at the interface correspond to the MOF-199 structure. No difference in the peak intensities is observed at the different times, which indicates that the formation of MOF-199 crystals is very fast. This rate of growth is greater than the one reported for the solvothermal synthesis of MOF-199.³⁵ When the inner [BTC] increases, the transition from spheroids to cubic crystals becomes too fast to be detected. On the other hand, when [BTC] decreases a hundred fold (*e.g.* 0.05 mM), the induction time increases to

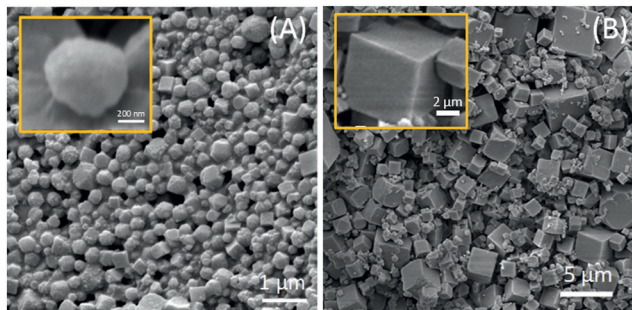


Fig. 3 SEM images exhibiting the growth of MOF-199 crystals at the interface region after 6 s (A) and after 10 s (B) for [BTC] = 5 mM and [Cu²⁺] = 300 mM.

hours. The only noticeable difference is in the size of the crystals that can be inferred from the broadened reflections obtained for the crystals of the short time reactions (Fig. S10[†]).

Conclusions

Metal-organic framework-199 (MOF-199) crystals were successfully synthesized *via* a reaction-diffusion process in a hydrogel matrix. Compared to the one-pot nucleation and growth techniques in homogeneous solution, which usually results in polydispersed MOF particles, our reaction-diffusion framework (RDF) allowed us to tune with ease their size and morphology by varying the temperature, the gel matrix and the concentrations and nature of the reagents. In addition, it is scalable and environmentally friendly. The RDF is currently being applied to synthesize other MOF and ZIF materials with different sizes and morphologies.

Acknowledgements

MH and MG gratefully acknowledge the funding provided by the American University of Beirut Research Board, the K. Shair Central Research Science Laboratory and the Lebanese National Council for Scientific Research. We thank Ms. Manal Ammar for her assistance in the experimental work.

Notes and references

- S. Kitagawa, *Chem. Soc. Rev.*, 2014, **43**, 5415–5418.
- H. Furukawa, K. E. Cordova, M. O’Keeffe and O. M. Yaghi, *Science*, 2013, **341**, 1230444.
- M. Eddaoudi, D. F. Sava, J. F. Eubank, K. Adil and V. Guillermin, *Chem. Soc. Rev.*, 2015, **44**, 228–249.
- H. Deng, S. Grunder, K. E. Cordova, C. Valente, H. Furukawa, M. Hmadeh, F. Gándara, A. C. Whalley, Z. Liu and S. Asahina, *Science*, 2012, **336**, 1018–1023.
- A. Coskun, M. Hmadeh, G. Barin, F. Gándara, Q. Li, E. Choi, N. L. Strutt, D. B. Cordes, A. M. Slawin and J. F. Stoddart, *Angew. Chem., Int. Ed.*, 2012, **51**, 2160–2163.
- W.-J. Li, M. Tu, R. Cao and R. A. Fischer, *J. Mater. Chem. A*, 2016, **4**, 12356–12369.
- B. T. Nguyen, H. L. Nguyen, T. C. Nguyen, K. E. Cordova and H. Furukawa, *Chem. Mater.*, 2016, **28**, 6243–6249.
- K. Manna, T. Zhang, F. X. Greene and W. Lin, *J. Am. Chem. Soc.*, 2015, **137**, 2665–2673.
- R. E. Hansen and S. Das, *Energy Environ. Sci.*, 2014, **7**, 317–322.
- U. Mueller, M. Schubert, F. Teich, H. Puetter, K. Schierle-Arndt and J. Pastre, *J. Mater. Chem.*, 2006, **16**, 626–636.
- S. L. James, C. J. Adams, C. Bolm, D. Braga, P. Collier, T. Friščić, F. Grepioni, K. D. Harris, G. Hyett and W. Jones, *Chem. Soc. Rev.*, 2012, **41**, 413–447.
- A. Martinez Joaristi, J. Juan-Alcañiz, P. Serra-Crespo, F. Kapteijn and J. Gascon, *Cryst. Growth Des.*, 2012, **12**, 3489–3498.
- T. Rodenas, I. Luz, G. Prieto, B. Seoane, H. Miro, A. Corma, F. Kapteijn, F. X. L. i Xamena and J. Gascon, *Nat. Mater.*, 2015, **14**, 48–55.
- L. Garzón-Tovar, A. Carné-Sánchez, C. Carbonell, I. Imaz and D. Maspoch, *J. Mater. Chem. A*, 2015, **3**, 20819–20826.
- K. Užarević, T. C. Wang, S.-Y. Moon, A. M. Fidelli, J. T. Hupp, O. K. Farha and T. Friščić, *Chem. Commun.*, 2016, **52**, 2133–2136.
- Z. Hu and D. Zhao, *Dalton Trans.*, 2015, **44**, 19018–19040.
- P. A. Bayliss, I. A. Ibarra, E. Pérez, S. Yang, C. C. Tang, M. Poliakoff and M. Schröder, *Green Chem.*, 2014, **16**, 3796–3802.
- Q. Yang, S. Vaesen, F. Ragon, A. D. Wiersum, D. Wu, A. Lago, T. Devic, C. Martineau, F. Taulelle and P. L. Llewellyn, *Angew. Chem., Int. Ed.*, 2013, **52**, 10316–10320.
- M. Sánchez-Sánchez, N. Getachew, K. Díaz, M. Díaz-García, Y. Chebude and I. Díaz, *Green Chem.*, 2015, **17**, 1500–1509.
- H. H. M. Yeung, Y. Wu, S. Henke, A. K. Cheetham, D. O’Hare and R. I. Walton, *Angew. Chem., Int. Ed.*, 2016, **55**, 2012–2016.
- Y. Wu, S. Henke, G. Kieslich, I. Schwedler, M. Yang, D. A. X. Fraser and D. O’Hare, *Angew. Chem., Int. Ed.*, 2016, **55**, 14081–14084.
- Z. Liu, H. Pan, G. Zhu, Y. Li, J. Tao, B. Jin and R. Tang, *Angew. Chem., Int. Ed.*, 2016, **55**, 12836–12840.
- S. R. Venna, J. B. Jasinski and M. A. Carreon, *J. Am. Chem. Soc.*, 2010, **132**, 18030–18033.
- B. Seoane, S. Castellanos, A. Dikhtiarenko, F. Kapteijn and J. Gascon, *Coord. Chem. Rev.*, 2016, **307**, 147–187.
- D. Zacher, J. Liu, K. Huber and R. A. Fischer, *Chem. Commun.*, 2009, 1031–1033.
- A. D. Katsenis, A. Puškarić, V. Štrukil, C. Mottillo, P. A. Julien, K. Užarević, M.-H. Pham, T.-O. Do, S. A. Kimber and P. Lazić, *Nat. Commun.*, 2015, **6**, 6662.
- P. Zhao, G. I. Lampronti, G. O. Lloyd, M. T. Wharmby, S. b. Facq, A. K. Cheetham and S. A. Redfern, *Chem. Mater.*, 2014, **26**, 1767–1769.
- G. A. Al Akhrass, M. Ammar, H. El-Rassy and M. Al-Ghoul, *RSC Adv.*, 2016, **6**, 3433–3439.
- D. Saliba, A. Ezzeddine, A.-H. Emwas, N. M. Khashab and M. Al-Ghoul, *Cryst. Growth Des.*, 2016, **16**, 4327–4335.

- 30 D. Saliba, A. Ezzeddine, R. Sougrat, N. M. Khashab, M. Hmadeh and M. Al-Ghoul, *ChemSusChem*, 2016, **9**, 800–805.
- 31 D. Saliba and M. Al-Ghoul, *CrystEngComm*, 2016, **18**, 8445–8453.
- 32 B. Zhang, J. Zhang, C. Liu, X. Sang, L. Peng, X. Ma, T. Wu, B. Han and G. Yang, *RSC Adv.*, 2015, **5**, 37691–37696.
- 33 J. Rahbani, A. R. Behzad, N. M. Khashab and M. Al-Ghoul, *Electrophoresis*, 2013, **34**, 405–408.
- 34 M. Dayeh, M. Ammar and M. Al-Ghoul, *RSC Adv.*, 2014, **4**, 60034–60038.
- 35 F. Millange, M. I. Medina, N. Guillou, G. Férey, K. M. Golden and R. I. Walton, *Angew. Chem., Int. Ed.*, 2010, **49**, 763–766.